Journal of Molecular Catalysis A: Chemical 423 (2016) 457–462

Contents lists available at ScienceDirect

Journal of Molecular Catalysis A: Chemical

journal homepage: www.elsevier.com/locate/molcata

Microstructure characters of Cu/ZnO catalyst precipitated inside microchannel reactor

Xin Jiang[a,*], Lu Zheng[a], Zhiyong Wang[a], Jiangang Lu[b]

[a] *College of Chemical and Biological Engineering, Zhejiang University, Hangzhou 310027, PR China*
[b] *State Key Laboratory of Industrial Control Technology, College of Control Science and Engineering, Zhejiang University, Hangzhou 310027, PR China*

ARTICLE INFO

Article history:
Received 1 June 2016
Received in revised form 20 July 2016
Accepted 25 July 2016
Available online 26 July 2016

Keywords:
Cu/ZnO catalyst
Microchannel reactor
Interaction between components
Intimate contact
Methanol synthesis

ABSTRACT

Cu/ZnO catalyst was prepared by co-precipitation method inside microchannel reactor and characterized by X-Ray diffraction (XRD), thermo gravimetric analysis (TGA), X-ray photoelectron spectroscopy (XPS), and high-resolution transmission electron microscopy (HRTEM). The XRD analysis of precursors demonstrates that, compared with the sample prepared by conventional batch reactor, more Zn^{2+} are incorporated into malachite structure, which is attributed to the relatively uniform distribution of Cu, Zn elements in initial precipitates caused by the excellent mixing performance of the microchannel reactor. Higher decomposition temperature of carbonate species trapped in the interfaces between CuO and ZnO and higher binding energy of $Cu2p_{3/2}$ indicate that sample prepared by the new reactor possess a stronger interface interaction, which derives from the more intimate contact between oxide components. This supposition is confirmed by the HRTEM images and the stronger interface interaction in the final reduced catalyst can improve catalytic performance on methanol synthesis.

1. Introduction

The well-known $Cu/ZnO/Al_2O_3$ catalyst has been widely employed in methanol synthesis from syngas for more than 40 years [1]. The binary Cu/ZnO catalyst system with a Cu:Zn ratio of 7:3 serves as a model for investigating the characters of the industrially applied ternary catalysts [2]. The synthesis process is started by co-precipitation reaction between aqueous solutions of metal nitrates and sodium carbonate. During the following ageing process, the initial products are transformed into crystalline precursor and correspondingly Cu^{2+} in malachite are gradually substituted by Zn^{2+}, forming the most active precursor, e.g. zincian malachite [3]. Active catalysts are obtained after the subsequent drying, calcination and reduction steps. The exposed Cu surface area and its intrinsic activity [4–6] are regarded as crucial factors with respect to the catalyst's performance. According to the previous literature [5], these two factors are deeply affected by the microstructure of final Cu/ZnO catalyst which is predetermined by the various synthesis parameters during the preparation process, and this phenomenon is termed as "chemical memory" of the system.

As well known, the precipitation process of Cu^{2+}, Zn^{2+} has a close relationship with the preparation parameters and styles [7]. In the normal concentration range of reagents, the precipitation reaction is a very fast process which is more rapid than the mixing process of reagents, resulting that the precipitation process occurs under inhomogenous mixing conditions [8]. Combined with the fact that Cu, Zn cations have inconsistent precipitation conditions and rates, the distribution of Cu, Zn elements in initial precipitate is inevitably inhomogeneous. It seems the redissolution and recrystallization [9] processes in subsequent ageing step could smooth and even eliminate the inhomogeneity, however, the pronounced "chemical memory" phenomenon indicates the initial uneven character has been taken into the microstructure of final catalyst.

The conventional preparation of Cu/ZnO catalyst is carried out in the batch reactors, in which even under "constant" precipitating conditions the chemical potential of reagents are neither spatially nor temporally homogenous [10]. Thus, the inconsistency on mixing and reaction conditions at different time and position inevitably bring about the uneven distribution of Cu, Zn elements and effects on the final microstructure of catalysts. Accordingly, to some extent the Cu surface area and its intrinsic activity are influenced.

In the past years, microchannel reactors have aroused extensive attention. They are widely used in preparing nanoparticles and can be regarded as continuous and steady state flow devices in which the reaction conditions do not change with the time. Furthermore,

---

* Corresponding author.
E-mail address: jiangx@zju.edu.cn (X. Jiang).

http://dx.doi.org/10.1016/j.molcata.2016.07.046
1381-1169/

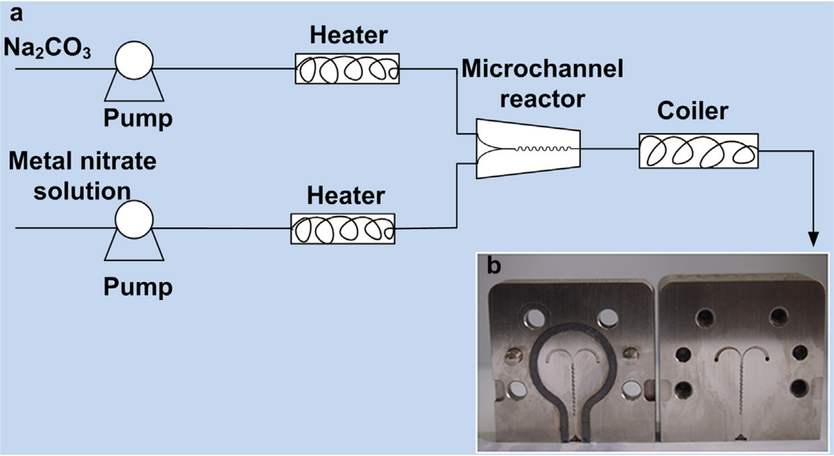

Fig. 1. (a) the scheme of preparation process by microchannel reactor (b) the photograph of inner flow channel of the microchannel reactor.

their tiny space and turbulence-inducing inner structure and configuration can significantly enhance and homogenize the mixing degree [11] in the channel. In this article we discuss the influences of these new features on the microstructure of precursors and catalysts.

2. Experiment methods

2.1. Catalyst preparation

The Cu, Zn (Cu/Zn molar ratio = 7/3) nitrate solution (0.4 M) and the aqueous Na_2CO_3 solution (0.4 M) were preheated to reaction temperature (70 °C), and then were simultaneously pumped into the microchannel reactor which has internal bas-relief structures to enhance the mixing degree of reagents (the scheme of preparation process and the image of inner flow channel of microchannel reactor are shown in Fig. 1). The mixed materials flowed through a coiled tube (20 m length, 2 mm ID) submerged in 70 °C water bath, and the pH value at outlet was regulated to set value by controlling the flow rate. After a 2 h ageing process, the obtained products were collected by filtration, and washed 6 times with deionized water. Subsequently, the samples were dried at 110 °C for 16 h followed by calcination at 350 °C in static air for 4 h. Finally the oxide components were reduced by 20 vol% H_2 in N_2 at 300 °C for 2 h.

For comparison, the conventional co-precipitation catalyst was prepared under the same conditions expect that precipitation process was conducted in a batch reactor with stir bar. Samples prepared by microchannel reactor and conventional batch reactor are respectively labeled as MR-X, BR-X, X represents for precursor, oxide, or catalyst.

2.2. Characterization method

X-ray powder diffraction (XRD) was performed on a X'Pert Pro MPD X-ray diffractometer using Cu-Kα radiation (λ = 0.15406 nm). Thermogravimetric analyses were performed on a Netzsch STA449 thermobalance (10 K/min, synthetic air). XPS measurements were performed using a Physical Electronics PHI-5400 ESCA work station equipped with a magnesium anode (Mg Kα = 1254 eV) at a power of 240 W (12 kV and 20 mA). A Tecnai G2 F20 microscope operated at 200 KV and equipped with a field emission gun was used for HRTEM. Cu surface area was measured by applying N_2O reactive frontal chromatography (RFC) [12].

Table 1
the lattice plane reflection characters of two precursors.

	$\bar{1}20$ (2θ)/°C	$\bar{1}21$ (2θ)/°C	d (20$\bar{1}$)/Å
BR-Precursor	32.15	33.15	2.761
MR-Precursor	32.40	33.29	2.744

2.3. Catalytic reaction

Catalysis activity measurement was performed in an up-flow tubular reactor (inner diameter 4 mm) made of stainless steel, loaded typically with 0.1 g of powder catalyst diluted with 1.0 g of quartz sand in 40–60 mesh. The reduced catalyst was maintained at 220 °C for 2 h in N_2 flowing at 40 ml/min. Then, syngas (H_2: CO = 2:1, with Ar as the internal standard, the specific proportions respectively are 64.2%, 32.1% and 3.7%) with a total flow rate at 60 ml/min (GHSV = 10276 h^{-1}) was switched in. The catalytic activity was determined under the following conditions: pressure 2 MPa, temperature range 220 °C–270 °C. After leaving the reactor, the organic products were analyzed by on-line GC (model 1102) equipped with a FID detector and the inorganic products were analyzed by on-line GC (model 9790) equipped with a TCD detector. The CO conversion was calculated from the formula: $X(CO) = (Mol(CO)_{in}/min \; - Mol(CO)_{out}/min)/Mol(CO)_{in} min \times 100\%$, $Mol(CO)_{in}$/min and $Mol(CO)_{out}$/min were respectively denoted the molar flow-rate of CO in inlet and outlet. Methanol production on per unit copper surface area was used to evaluate the catalytic performance.

3. Results and discussion

3.1. Microstructure characterization of precursors

The XRD patterns of the precursors prepared by two methods were shown in Fig. 2. All the marked peaks belong to the reflections of zincian malachite (JCPDS-PDF 41-1390). As shown in the figure, the reflections of 20$\bar{1}$, 21$\bar{1}$ lattice planes of zincian malachite in the MR-Precursor shift towards higher angles and the corresponding d-spacing of 20$\bar{1}$ reflection has a lower value (see Table 1). Pointed in the literatures, the observed phenomenon is indicative of more Cu^{2+} (d^9, Jahn-Teller distorted coordination preferred) substituted by Zn^{2+} [13] (d^{10}, no Jahn-Teller distortion), which would exert a larger contraction on the Jahn-Teller distortions of MO_6 octahedral in the malachite structure and thus lower the d-spacing value of 20$\bar{1}$ reflection. Estimated by the established function [9] between the amount of incorporated Zn^{2+} and d-spacing value, the Zn content in

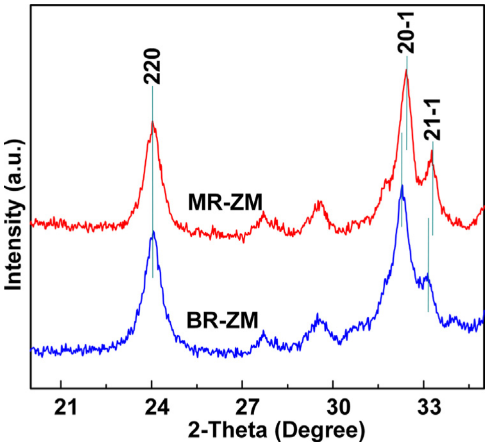

Fig. 2. the XRD patterns of precursors prepared by two methods.

the zincian malachite prepared by microchannel reactor is 28.4%, while for the conventional co-precipitation method the value is 23.8%. As the Zn content incorporated into the malachite depends heavily on the preparation parameters and styles [9,14], we deduce that the gap comes from different courses of precipitation process in the two reactors.

As a very fast process, the precipitation process of Cu^{2+} and Zn^{2+} proceeds before the homogeneity of the reagents has been established [15]. Thus, concentration and pH gradients of reactants at the micro-level cannot be avoided before the precipitation reaction process ends. Due to the fact that the precipitation behaviors of Cu^{2+} and Zn^{2+} are inconsistent [16] (e.g. the starting pH of Cu^{2+} is about 3 and Zn^{2+} near pH 5) and seriously affected by pH, the existing gradient of pH causes an inconsistent precipitation and uneven distribution of Cu, Zn elements in initial precipitation product. For the microchannel reactor, the tiny space and turbulence-inducing channel structures can relatively enhance and homogenize the mixing degree inside the reactor. While in the conventional batch reactor, there is a remarkable difference in the mixing performance from point to point and weaker turbulent degree inevitably appears in the regions far away from the stirring center. The lower turbulence aggravates the inhomogeneous distribution of Cu and Zn elements and then suppresses the incorporation process of Zn^{2+} in the ageing step. Therefore, the content of Zn^{2+} incorporating into zincian malachite in the BR-Precursor is lower than that in the MR-Precursor.

Fig. 3 is the TGA profiles of precursors. Both samples show the typical thermal behaviors of Cu, Zn mixed precursors. BR-Precursor exhibits two weight loss steps at 327 and 427 °C, while MR-Precursor at 331 and 472 °C. According to the literature [17], the first weight loss step is owned to the simultaneous dehydration and decarbonation process. During this step, the interfaces and grain boundaries between CuO and ZnO are formed. With respect to the higher temperature weight loss step, it exclusively results from the decomposition of carbonate species (HT-CO_3^{2-}) trapped in the interfaces between CuO and ZnO. As claimed in literatures [10,17], the higher temperature of HT-CO_3^{2-} is an indicator of stronger interaction across interfaces between CuO and ZnO. Accordingly, a stronger interface contact exists in the MR-Oxide microstructure.

Estimated from Fig. 3, the fraction of carbonate species decomposed at higher temperature in the total weight loss is 12.3% for BR-Precursor and 22.1% for MR-Precursor. Confirmed by many experiments, the abundance of HT-CO_3^{2-} has a positive correlation with the amount of interfaces and grain boundaries [18] which is determined by the Zn^{2+} content in the zinc malachite. Hence, more amount of HT-CO_3^{2-} in the MR-Precursor malachite structure is the function of more incorporated Zn^{2+}, which is correspond with the description above.

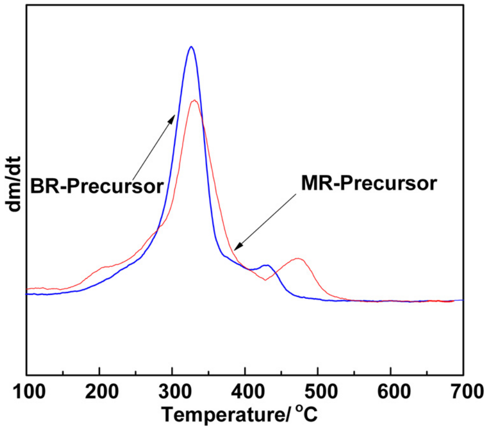

Fig. 3. the TGA profiles of precursors prepared by two methods.

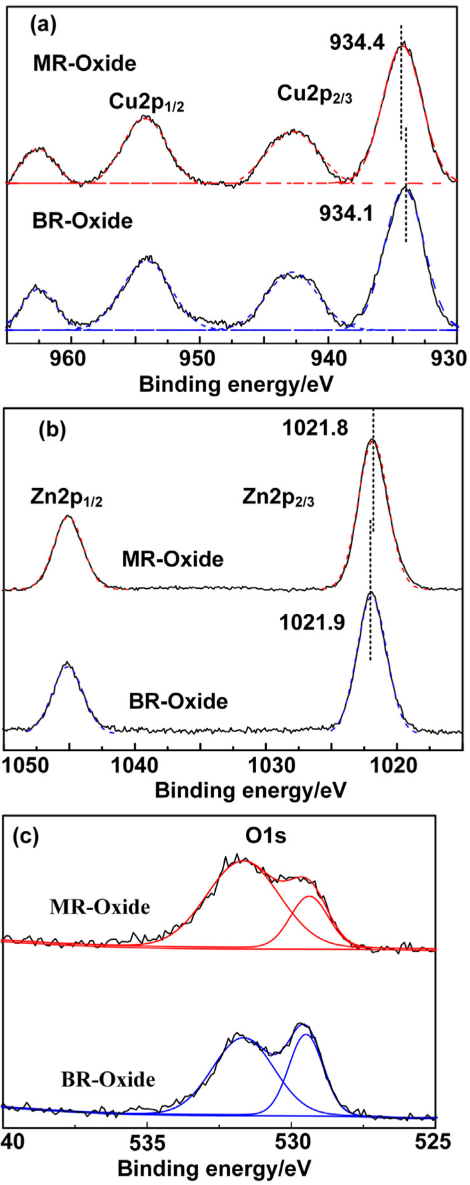

Fig. 4. the X-ray photoelectron spectra of the Oxide samples (a) the XPS spectra of Cu2p, (b) the XPS spectra of Zn2p, (c) the XPS spectra of O1s.

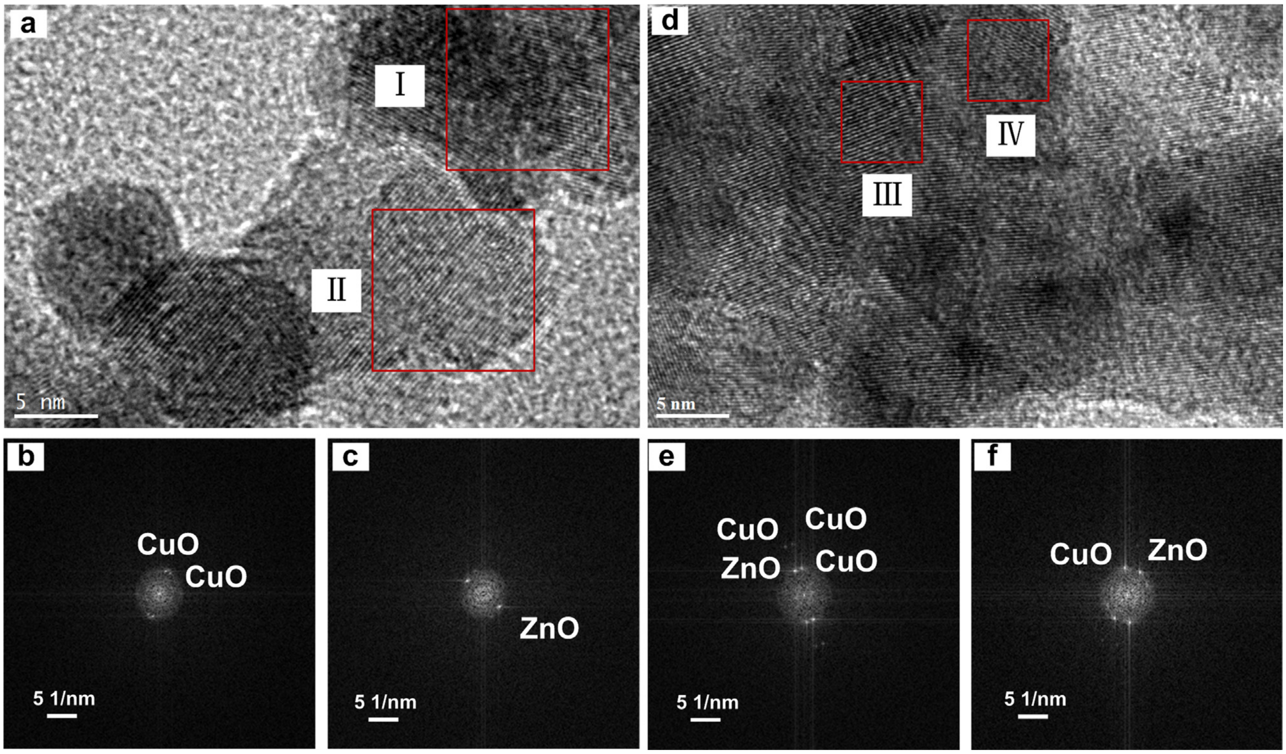

Fig. 5. HRTEM images of two samples (a) BR-Oxide, (b) FFT pattern of area I, (c) FFT pattern of area II, (d) MR-Oxide, (e) FFT pattern of area III, (f) FFT pattern of area IV.

3.2. *Microstructure characters of oxide samples*

Fig. 4 shows XPS spectra of core level Cu2p, Zn2p, O1 s and these data are fitted with Gaussian function. Proved by the peak positions of Cu2p$_{3/2}$ binding energy (Fig. 4(a), 934.4 eV, 934.1 eV) as well as by the presence of intensive shake-up satellites in the range of 940–945 eV [19,20], both calcined samples only contained Cu^{2+} at the surface. Compared with the binding energy of Cu2p3/2 (933.6 eV) in the pure CuO, both samples have a significant shift towards high values, which is caused by the interaction between CuO and ZnO [21]. As can be seen from Fig. 4(b), the binding energy of Zn2p$_{3/2}$ of MR-Oxide and BR-oxide are respectively 1021.9 eV and 1021.8 eV. Compared with the binding energy of Zn2p$_{3/2}$ (1022.2 eV) in the pure ZnO, both samples have a shift towards lower values which is also aroused by the interaction between CuO and ZnO. It was reported that higher value of the Cu^{2+} binding energy and lower value of Zn^{2+} binding energy corresponds to stronger interaction between CuO and ZnO [21,22]. The obtained results further confirm the so-called stronger interface in the MR-Oxide microstructure.

As shown in Fig. 4(c), the O1s-spectra of both samples are consisted of two peaks. Described in the literature [20], the peak located at 529.5 eV is assigned to the lattice oxygen in CuO and ZnO and the other peak located at 531.6 eV is assigned to the residual carbonate species in oxide samples (HT-CO$_3{}^{2-}$). Calculated from the corresponding peak area, the amount of residual carbonate species in MR-Oxide is 1.8 times than that in BR-Oxide, which is in good agreement with characterization results (the value is 1.9) in Fig. 3.

Fig. 5 is the HRTEM images of two samples accompanied with diffraction patterns of the selected areas via FFT method. Similar to what has been presented by other researchers [5], the micromorphology of BR-Oxide shows a feature that CuO particles are separated by some individual ZnO particles, forming a porous framework of particles. Whereas, in the MR-Oxide, the diffraction patterns of lattice planes of CuO and ZnO can be simultaneously found in a small enough area, individual separated oxide particles are hardly detected, which could be the impact of homogeneous distribution of Cu, Zn elements. Thus, we speculate the more intimate interface contact and better inter-dispersion between oxide components may be the direct reason for enhanced interface interaction in the MR-Oxide microstructure.

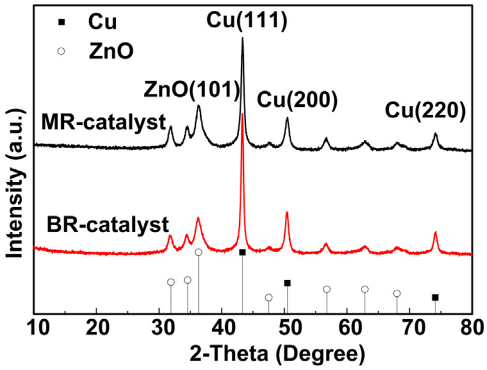

Fig. 6. XRD patterns of the two reduced catalysts.

3.3. *Reduced catalysts and catalytic performance*

Fig. 6 shows the XRD patterns of the final reduced Cu/ZnO catalysts. All diffraction peaks can be attributed to Cu (JCPDS-PDF 4-836) and ZnO (JCPDS-PDF 36-1451) phases. The sizes of Cu and ZnO crystallites are calculated by Scherrer Formula according to the corresponding reflection line (Cu (111), $2\theta = 43.297^\circ$, ZnO (101), $2\theta = 36.252^\circ$) and the values don't show obvious changes. For the convenience of the following calculating process, the sizes of Cu crystallites are listed in Table 2. The corresponding Cu surface area (SA$_{Cu}$) is measured by applying N$_2$O reactive frontal chromatography. The interface ratios[17] (IFR) (i.e. the fraction of Cu particles not exposed to the gas atmosphere but present as interface to ZnO phase) equal to the ratio of measured SA$_{Cu}$ to the theoretically avail-

Table 2
the performance parameters of two reduced catalysts.

	d(Cu^0) nm	SA_{Cu} $m^2\,g^{-1}$	IFR %	Lattice strain	Catalytic activities mmol $m^{-2}{}_{Cu}\,h^{-1}$
BR-Reduced	13.4	6.5	80.1	0.181%	126
MR-Reduced	13.2	4.0	88.1	0.241%	260

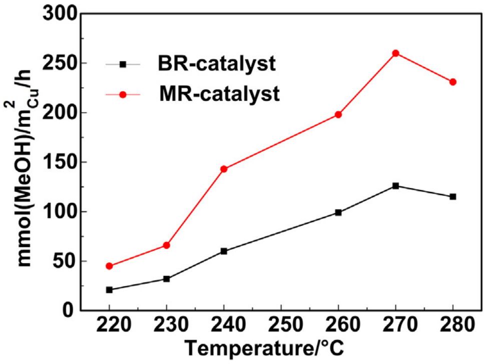

Fig. 7. the Catalytic activities of two reduced catalysts at different reaction temperature.

able Cu surface calculated from the XRD determined average Cu crystallites sizes. As can be seen from the calculated results listed in the Table 2, the MR-Catalyst sample has a lower Cu surface area but a higher IFR which manifests that the Cu particles in MR-catalyst have a stronger interface interaction with the ZnO particles [5]. This is in agreement with the stronger interface interaction in the MR-Oxide microstructure, demonstrating that the enhanced interface interaction survives after the reduction process.

In order to compare their catalytic performance both reduced catalysts were tested in the methanol synthesis reaction, the results are shown in Fig. 7. The catalytic activities of both samples initially increase with the reaction temperature and the maximum catalytic activities of per unit copper surface area (the values are given in Table 2) are obtained at 270 °C. As the equilibrium conversion for methanol synthesis at 280 °C (2 MPa, H_2:CO = 2:1) is only 7.4% (the conversions of two samples are respectively 6.3% and 5.1% which are not very far from equilibrium value), the catalytic activities measured at this temperature show a downward trend.

Obviously, the activity of MR-catalyst is about twice as large as the value of BR-catalyst. Considering of the characterizations mentioned above, it is reasonable to assume that the intrinsic activity of exposed Cu surface in MR-catalyst has been improved by the presented stronger Cu-ZnO interface interaction which is useful for the stabilization of the strained and defective form of Cu particles [23]. Thus, high value of Cu lattice strain and abundance of Cu defects identified as symbols of high intrinsic activity [23,24] can be expected. It is worth mentioning that the CO conversion of MR-catalyst is not very far from the equilibrium conversion (10.3%) under our reaction conditions (2 MPa, 270 °C, H_2: CO = 2:1), demonstrating that the intrinsic activity of MR-catalyst has been substantially enhanced.

Williamson-Hall method was used to calculate the values of Cu lattice strain (Fig. 8) in two samples [25,26]. The method assumes that if the XRD patterns can be satisfactorily fitted by Lorentz function, the total physical broadening of XRD pattern is a linear addition of ‘size’ and ‘strain’ effects. For isotropic effects, the plot of $\beta\cos(\theta)/\lambda$ versus $2\sin(\theta)/\lambda$ should results in a straight line. The mean value of lattice strain (See Table 2) equals the half of the slope in Fig. 8. As expected, the value of Cu lattice strain has improved a lot in the MR-Catalyst, which can be regarded as a supplement evidence for the described higher intrinsic activity in the MR-Catalyst.

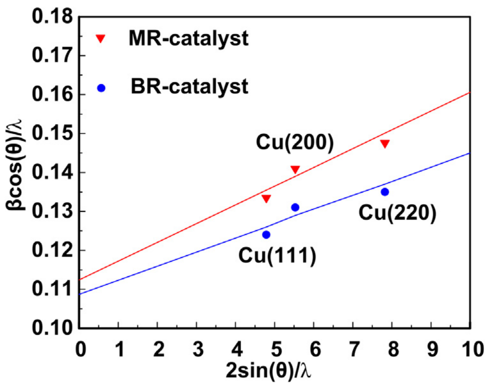

Fig. 8. Williamson-Hall plots of two reduced catalysts.

4. Conclusion

Compared with the conventional batch reactor, the characters of flow and mixing in the microchannel reactor can bring a more homogenous Cu, Zn distribution in the initial precipitation products. As a result, more Zn^{2+} ions are incorporated into the malachite structure confirmed by higher reflection angels and lower d($20\bar{1}$) spacing of zincian malachite. In the following calcination step, a more intimate contact between the oxide components improves the interface interaction, which is supported by DTG, XPS and HRTEM characterization methods. The stronger interface interaction survives in the reduced catalyst and then enhances the intrinsic activity for methanol synthesis.

Acknowledgements

Financial support from National Science Foundation of China Grants (Contract 21276223), the Chinese Key Technology R&D Program (2010AA064905) and the Program for Zhejiang Leading Team of Science & Technology Innovation (Contract 2009R50020) are gratefully acknowledged.

References

[1] J.-L. Li, T. Inui, Appl. Catal. A 137 (1996) 105–117.
[2] Malte Behrens, Stefan Kißner, Frank Girsgdies, Igor Kasatkin, Felix Hermerschmidt, Katharina Mette, Holger Ruland, Martin Muhler, Robert Schlögl, Chem. Commun. 47 (2011) 1701–1703.
[3] M. Behrens, J. Catal. 267 (2009) 24–27.
[4] P. Munnik, M. Wolters, A. Gabrielsson, S.D. Pollington, G. Headdock, J.H. Bitter, P.E. de Jongh, K.P. de Jong, J. Phys. Chem. C 115 (2011) 14698–14706.
[5] M. Behrens, A. Furche, I. Kasatkin, A. Trunschke, W. Busser, M. Muhler, B. Kniep, R. Fischer, R. Schlögl, ChemCatChem 2 (2010) 816–818.
[6] Melanie Kurtz, Natalia Bauer, Christoph Büscher, Hagen Wilmer, Olaf Hinrichsen, Ralf Becker, Stefan Rabe, Klaus Merz, Matthias Driess, Roland A. Fischer, Martin Muhler, Catal. Lett. 92 (2004) 49–52.
[7] M. Behrens, R. Schlögl, Z. Anorg, Allg. Chem. 639 (2013) 2683–2695.
[8] Martain A.J. Harting, Nikolas Jacobsen, Wolfgang Peukert, Chem. Eng. Sci. 109 (2014) 158–170.
[9] S. Zander, B. Seidlhofer, M. Behrens, Dalton Trans. 41 (2012) 13413–13422.
[10] M. Schur, B. Bems, A. Dassenoy, I. Kassatkine, J. Urban, H. Wilmes, O. Hinrichsen, M. Muhler, R. Schlögl, Angew. Chem. Int. Ed. 42 (2003) 3815–3817.
[11] X. Yao, Y. Zhang, L. Du, J. Liu, J. Yao, Renew. Sustain. Energy Rev. 47 (2015) 519–539.
[12] G.C. Chinchen, C.M. Hay, H.D. Vandervell, K.C. Waugh, J. Catal. 103 (1987) 79–87.
[13] M. Behrens, F. Girgsdies, Z. Anorg, Allg. Chem. 636 (2010) 919–927.
[14] B. Bems, M. Schur, A. Dassenoy, H. Junkes, D. Herein, R. Schlögl, Chem. Eur. J. 9 (2003) 2039–2052.
[15] A. Nagaki, M. Togai, S. Suga, N. Aoki, K. Mae, J. Yoshida, J. Am. Chem. Soc. 127 (2005) 11666–11675.

[16] M. Behrens, D. Brennecke, F. Girgsdies, S. Kißner, A. Trunschke, N. Nasrudin, S. Zakaria, N.F. Idris, S.B.A. Hamid, B. Kniep, R. Fischer, W. Busser, M. Muhler, R. Schlögl, Appl. Catal. A 392 (2011) 93–102.
[17] S. Kühl, M. Friedrich, M. Armbrüster, M. Behrens, J. Mater. Chem. 22 (2012) 9632–9638.
[18] M. Behrens, F. Girgsdies, A. Trunschke, R. Schlögl, Eur. J. Inorg. Chem. 7 (2009) 910–921.
[19] Jong Wook Bae, Suk-Hwan Kang, Yun-Jo Lee, Ki-Won Jun, App. Catal. B 90 (2009) 426–435.
[20] D.A. Svintsiskiy, A.P. Chupakhin, E.M. Slavinskaya, O.A. Stonkus, A.I. Stadnichenko, J. Mol. Catal. A: chem. 368–369 (2013) 95–106.
[21] D. Ji, W. Zhu, Z. Wang, G. Wang, Catal. Commun. 8 (2007) 1891–1895.
[22] G. Fabio, G. Petrini, J. Catal. 90 (1984) 106–112.
[23] S. Zander, E.L. Kunkes, M.E. Schuster, J. Schumann, G. Weinberg, D. Teschner, N. Jacobsen, R. Schlögl, M. Behrens, Angew. Chem. Int. Ed. 52 (2013) 6536–6540.
[24] I. Kasatkin, P. Kurr, B. Kniep, A. Trunschke, R. Schlögl, Angew. Chem. Int. Ed. 46 (2007) 7324–7327.
[25] T. Kandemir, I. Kasatkin, F. Girgsdies, S. Zander, S. Kühl, M. Tovar, R. Schlögl, M. Behrens, Top. Catal. 57 (2014) 188–206.
[26] B.L. Kniep, T. Ressler, A. Rabis, F. Girgsdies, M. Baenitz, F. Steglich, R. Schlögl, Angew. Chem. Int. Ed. 43 (2004) 112–115.